ISSN 1063-7826, Semiconductors, 2014, Vol. 48, No. 8, pp. 1051–1062. © Pleiades Publishing, Ltd., 2014.

AMORPHOUS, VITREOUS, AND ORGANIC SEMICONDUCTORS

Theoretical Studies on Dimerization Reactions of 4, 7-diphenyl-1,10-phenanthroline (BPhen) and Bathocuproine (BCP) in Organic Semiconductors[1]

Fahimeh Shojaie

Department of Photonics, Graduate University of Advanced Technology, Kerman, Iran

e-mail: fahimeh_shojaie@yahoo.com

Submitted September 11, 2013; accepted for publication, November 5, 2013

Abstract—The dimerization reactions of 4, 7-diphenyl-1,10-phenanthroline (BPhen) and bathocuproine (BCP) were studied theoretically. In this work, the molecular geometries, BPhen and BCP monomers, positively charged BPhen and BCP intermediates, and BPhen and BCP dimers were calculated in neutral state at different levels of ab initio methods for the dimerization reactions. The molecular geometries of the BPhen and the BCP monomers and their dimers in their cationic and anionic states were optimized using the B3LYP/6-31G(*d*) method. The π orbitals interactions in the phenyl groups are responsible for the shortening of the C_6–N_1 and C_7–N_1 bond distances in BPhen and BCP dimers. The large difference between the reorganization energy components of BCP dimer for hole transport process is due to larger energy required to reorganize $C_5C_4N_2C_6$ and $C_8C_1N_1C_7$ angles. The methyl groups and the phenyl rings act as sterically hindering groups in the BPhen and BCP dimers. In contrast to BPhen dimer where its electron hopping rate is less than BPhen monomer, the magnitude of electron hopping rate of BCP dimer is 12 times higher than BCP monomer.

DOI: 10.1134/S1063782614080223

1. INTRODUCTION

It has been demonstrated that organic light-emitting diodes (OLEDs) can be used for flat panel displays and solid-state lighting applications [1, 2]. Intensive researches have been carried out to find materials with high light-emitting efficiencies, high thermal stabilities and good amorphous film formation properties [3, 4]. The optoelectronic properties of OLED devices depend on the highest occupied molecular orbital (HOMO) and the lowest unoccupied molecular orbital (LUMO) energy levels and electron and hole mobility [3, 4].

Sebastian et al. studied photochemical reactions of different organic semiconductor materials commonly used in OLEDs by means of laser desorption/ionization time-of-flight mass spectrometry (LDI–TOF–MS) technique [5]. Theses photochemical reactions were induced in the organic semiconductor materials by UV-laser light irradiation under the influence of a positive bias voltage [5]. The analysis of LDI–TOF–MS spectra allows an additional understanding of the underlying degradation mechanisms, which may occur in electrically driven organic semiconductor devices [5]. Sebastian et al. studied possible reaction pathways and the different stages of dimerization of the well-known electron transport material BPhen and compared these to the results with its analog BCP, showing the degradation of the two materials under hole transporting conditions [5]. Several studies have been carried out over the past years revealing different degradation mechanisms for OLEDs [6–13].

Sebastian et al. applied laser desorption/ionization (LDI) technique to create the dimerization reactions of the BPhen and BCP monomers and showed these reactions occurred via the pathway that is shown in Fig. 1 [5].

The pathway for the dimerization reactions in both cases (BPhen and BCP) consists of two reaction steps. The first step is a neutral monomer (BPhen, BCP) addition to an excited positively charged monomer molecule ($BPhen^{*+}$, BCP^{*+}) and the formation of the intermediates (IM1, IM2). The second step is the production of products (P1, P2). The reaction pathways in Fig. 1 can be written in short forms as follows:

$$\text{BPhen} + \text{BPhen}^{*+}(R1) \longrightarrow \text{IM1}^{+} + \text{H}^{*}(\text{IM1}) \longrightarrow \text{D1} + \text{H}^{+} + \text{H}^{*}(\text{P1}), \quad \text{Reaction (1)}$$

$$\text{BCP} + \text{BCP}^{*+}(R2) \longrightarrow \text{IM2}^{+} + \text{H}^{*}(\text{IM2}) \longrightarrow \text{D2} + \text{H}^{+} + \text{H}^{*}(\text{P2}), \quad \text{Reaction (2)}$$

where the D1 and the D2 are the BPhen and the BCP dimers respectively.

The thermodynamic properties of these reaction pathways were calculated in the standard states using a

[1] The article is published in the original.

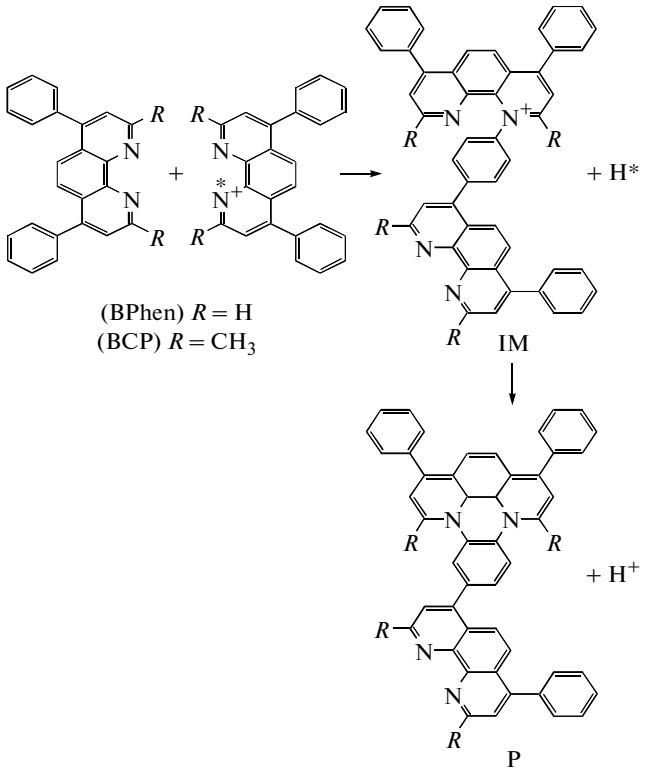

Fig. 1. Dimerization reactions of BPhen ($R = H$) and BCP ($R = CH_3$) after a short laser pulse excitation and an applied positive high voltage by LDI experiments [5].

combination of quantum mechanical computations performed by the Gaussian 03 program [14] at the HF/3-21G*, HF/6-31G(*d*), B3LYP/3-21G* and B3LYP/6-31G(*d*) levels. Molecular orbital (MO) calculations were performed at the same levels too.

The molecular geometries of the monomers (BPhen, BCP) and their dimers (D1 and D2) in their cationic and anionic states were optimized by the Density functional theory (DFT) modelling method, DFT/B3LYP, using the 6-31G(*d*) basis set. The ionization potentials, electron affinities and reorganization energies of the above compounds were calculated using B3LYP/6-31G(*d*) method. In this paper, we present DFT calculations to determine the hopping transport rate of electron and hole. The charge carrier transport is an important factor for developing high efficiency OLED materials.

2. COMPUTATIONAL METHODS

The molecular geometries of the monomers (BPhen, BCP), positively charged intermediates ($IM1^+$, $IM2^+$) and the dimers (D1, D2) were optimized at the HF/3-21G*, HF/6-31G(*d*), B3LYP/3-21G* and B3LYP/6-31G(*d*) levels of ab initio method.

Vibrational frequencies of these compounds, also calculated at the same levels of ab initio method, have been used to determine zero-point energy (ZPE), entropy, free energy and enthalpy. The energy of the compounds excited state was calculated by the time-dependent self–consistent–field (TD–SCF) method [15]. The ionization potentials, electron affinities and reorganization energies of these compounds have been calculated at B3LYP/6-31G(*d*) level. All calculations were carried out using the Gaussian 03 program.

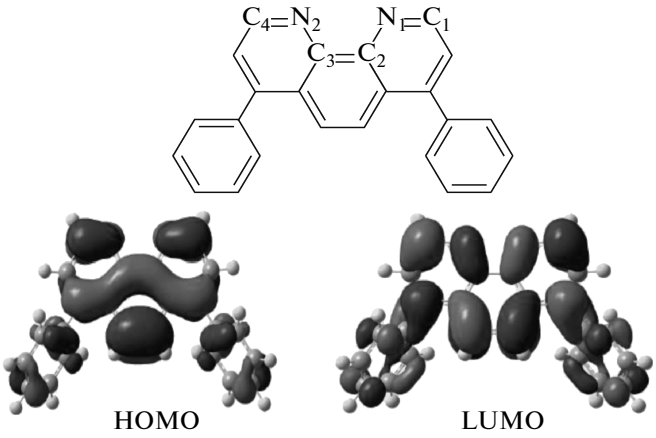

Fig. 2. The structure of the BPhen in neutral state and the electron density isocontours of HOMO and LUMO using the DFT/B3LYP method with the 6-31G(*d*) basis set.

3. RESULTS AND DISCUSSION

3.1. Optimized Molecular Geometries

The structures and the electron density isocontours of HOMO and LUMO of the BPhen and BCP monomers, positively charged intermediates IM1 and IM2 and the dimers D1 and D2 are shown in Fig. 2–7. The optimized molecular geometries, the energies of frontier molecular orbitals (E_{LUMO}, E_{HOMO}) and the HOMO and LUMO energy gaps ($\Delta E = E_{LUMO} - E_{HOMO}$) these structures are shown in Tables 1–6.

Tables 1–6 show that the molecular geometries that were calculated with different basis sets are only slightly different. The electron density isocontours (Figs. 3 and 6) show that in both $IM1^+$ and $IM2^+$ intemediates, the π orbitals of the star labeled rings make a large contribution to their LUMO energies whereas these π orbitals do not contribute to their HOMO energies. In case of the D1 and D2 dimers, the density isocontours show that the π orbitals of the star labeled rings make major contributions to both LUMO and HOMO energies of the dimers (Tables 3 and 6). When an H^+ is removed from $IM1^+$ and $IM2^+$, C_6–N_1 and C_7–N_1 bond distances are shortened by 1.787 and 1.692 Å, respectively. The π orbitals interactions in the phenyl groups are responsible for the shortening of the C_6–N_1 and C_7–N_1 bond distances. Since one of the most accurate theoretical techniques is the density functional theory which can be applied to most sys-

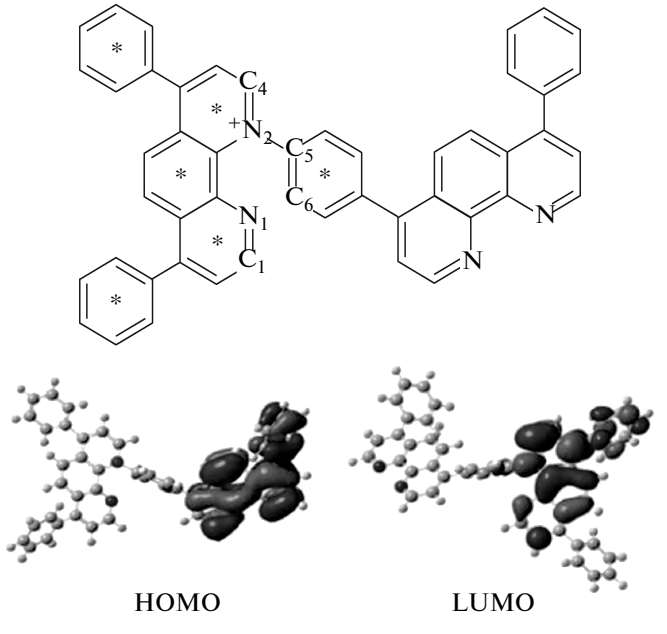

Fig. 3. The structure of the $IM1^+$ in neutral state and the electron density isocontours of HOMO and LUMO using the DFT/B3LYP method with the 6-31G(*d*) basis set.

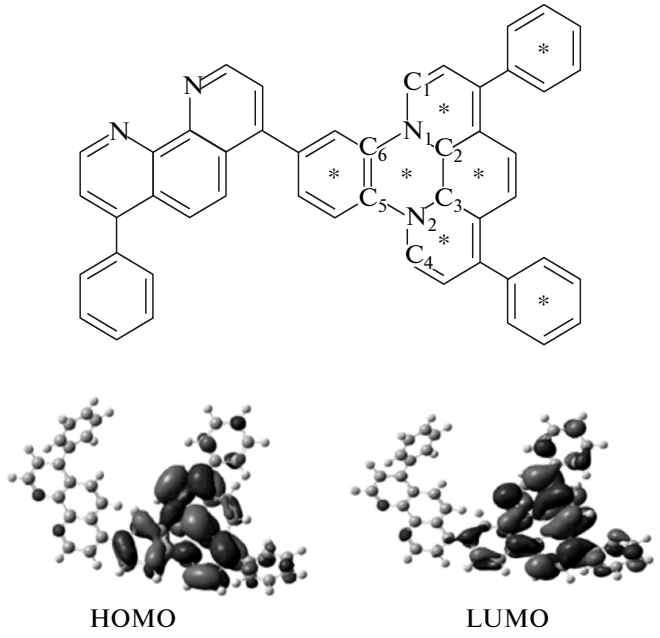

Fig. 4. The structure of the D1 in neutral state and the electron density isocontours of HOMO and LUMO using the DFT/B3LYP method with the 6-31G(*d*) basis set.

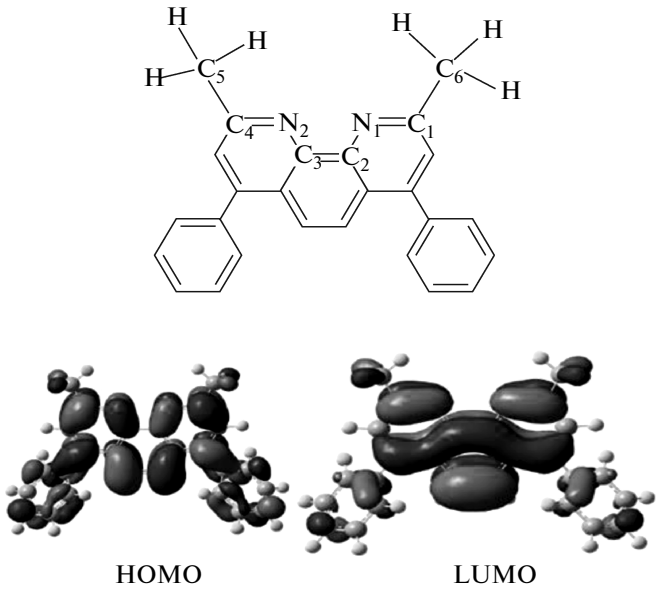

Fig. 5. The structure of the BCP in neutral state and the electron density isocontours of HOMO and LUMO using the DFT/B3LYP method with the 6-31G(*d*) basis set.

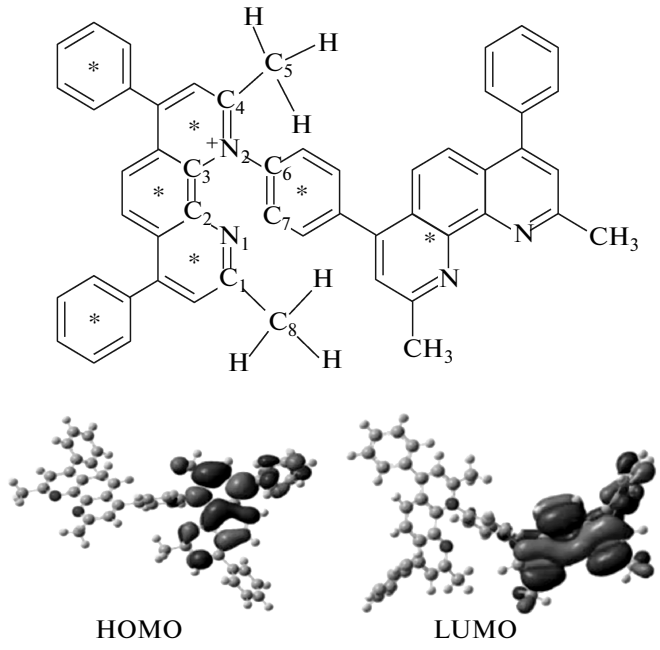

Fig. 6. The structure of the $IM2^+$ in neutral state and the electron density isocontours of HOMO and LUMO using the DFT/B3LYP method with the 6-31G(*d*) basis set.

tems and allows the structure to be efficiently optimized [16–18], so B3LYP/6-31G(*d*) clearly provide better results for organic molecules. BPhen has energy gap 3.4 eV [19] and BCP has 4.2 eV [20], as shown in Table 1 and 4, these energies by B3LYP/6-31G(*d*) are in better agreement with these values.

The geometrical variations in the monomers and the dimers can be noticed from their HOMO and LUMO. The dimers have the higher HOMO and the lower LUMO levels than their monomers. The ΔE values of the dimers are lower than their monomers counterparts. The $IM1^+$ and the $IM2^+$ act as electron traps

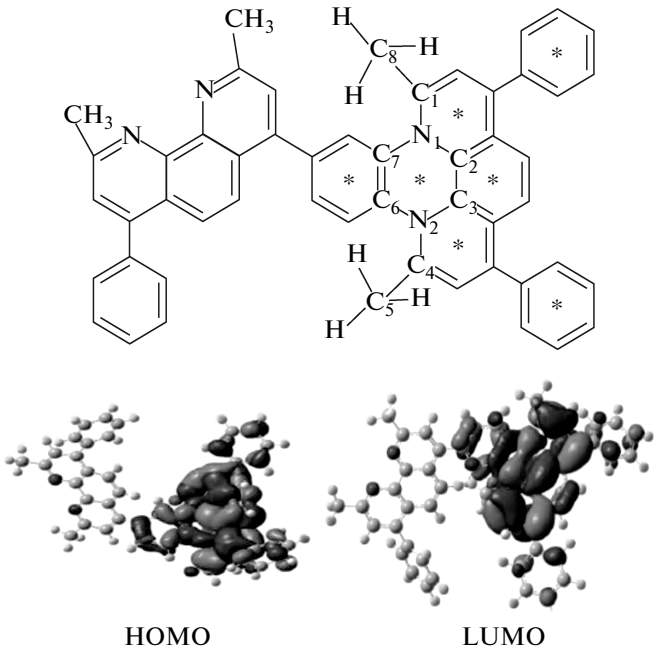

Fig. 7. The structure of the D2 in neutral state and the electron density isocontours of HOMO and LUMO using the DFT/B3LYP method with the 6-31G(*d*) basis set.

because they have the lowest HOMO levels. The HOMO energies of the dimers are larger than the HOMO energies of the monomers. The LUMO energies of the intermediates are smaller than the LUMO energies of both the monomers and the dimers. The geometrical variations in the BPhen and BCP in their cationic and anionic states can be seen by comparing their HOMO and LUMO energies (See Tables 1, 4, 7 and 8).

The HOMO and LUMO of the rings make major contributions to the large geometrical variations in the BPhen and BCP. The orbitals of nitrogen atoms contribute to the formation of both the HOMO and LUMO antibondings. The HOMO and LUMO antibondings strongly interact with the π orbitals of the rings. The lengthening of C_1–N_1 and C_4–N_2 and the shortening of C_2–N_1 and C_3–N_2 bond distances in both cationic and anionic states are expected by the molecular orbitals of BPhen and BCP. The presence of the methyl groups in the BCP has negligible effect on the HOMO and LUMO.

Tables D1 (A), D1 (B), D2 (A) and D2 (B) compare some of the bond lengths and torsional angles of the D1 and the D2 dimers in neutral (Tables 3 and 6), cationic and anionic states (Tables 9 and 10).

3.2. Reorganization Energy

The charge transport properties of organic materials are well described in the formulism of Gaussian disorders by Bassler and co-worker [21]. Energy and position disorders are two key parameters in this formulism [22]. For designing suitable hole or electron transporting materials, it is difficult to relate these two disorder parameters to molecular properties [22]. The measured hole and electron mobility of oligoacene crystals show a band hopping transition occurring at about room temperature [23].

Hopping of hole or electron can be described as an electron transfer (ET) from a charged, relaxed unit to an adjacent neutral unit and the mobility depends on the electron transfer rate [23]. The transfer of hole and electron can be described as a self-exchange reaction (3) [23]

$$M^{\pm} + M \longrightarrow M + M^{\pm}. \qquad \text{Reaction (3)}$$

Where $M^{\pm}$ refers to the molecule in a cationic or anionic state and M indicates the adjacent molecule in

Table 1. Molecular geometry, bond distances, bond angles, torsional angles, the calculated HOMO and LUMO energies and energy gaps of BPhen in neutral state

Bond/angle name	HF/3-21G*	HF/6-31G(*d*)	B3LYP/3-21G*	B3LYP/6-31G(*d*)
C_2–C_3, Å	1.451	1.461	1.455	1.461
N_1–N_2, Å	2.744	2.711	2.743	2.717
C_1–N_1, Å	1.309	1.297	1.332	1.321
C_2–N_1, Å	1.342	1.339	1.359	1.352
C_3–N_2, Å	1.342	1.339	1.359	1.352
C_4–N_2, Å	1.309	1.297	1.332	1.321
$N_1C_2C_3N_2$, deg	0.000	0.000	–0.000	0.000
$C_1N_1C_2$, deg	119.57	118.38	118.29	117.74
$C_3N_2C_4$, deg	119.57	118.38	118.29	117.74
E_{LUMO}, eV	2.2653	2.3507	–1.4854	–1.4658
E_{HOMO}, eV	–8.2147	–7.9584	–6.1447	–5.9758
ΔE, eV	10.4800	10.3091	4.6593	4.50995

Table 2. Molecular geometry, bond distances, bond angles, torsional angles, the calculated HOMO and LUMO energies and energy gaps of $IM1^+$ in neutral state

Bond/angle name	HF/3-21G*	HF/6-31G(*d*)	B3LYP/3-21G*	B3LYP/6-31G(*d*)
C_2–C_3, Å	1.449	1.457	1.448	1.454
N_1–N_2, Å	2.839	2.837	2.834	2.837
C_1–N_1, Å	1.306	1.296	1.331	1.321
C_2–N_1, Å	1.339	1.337	1.353	1.348
C_3–N_2, Å	1.372	1.337	1.385	1.388
C_4–N_2, Å	1.338	1.329	1.359	1.350
C_5–N_2, Å	1.447	1.465	1.484	1.470
C_6–N_1, Å	3.159	3.188	3.199	3.210
$N_1C_2C_3N_2$, deg	–2.317	–8.940	–5.179	–9.654
$C_1N_1C_2$, deg	120.26	118.99	118.93	118.27
$C_3N_2C_4$, deg	120.88	120.47	120.84	120.61
$C_5N_2C_3$, deg	125.58	125.98	125.38	125.64
E_{LUMO}, eV	–2.2590	–2.2590	–5.809	–5.6998
E_{HOMO}, eV	–9.6449	–9.6449	–7.7284	–7.6275
ΔE, eV	7.3858	7.3858	1.9194	1.9276

Table 3. Molecular geometry, bond distances, bond angles, torsional angles, the calculated HOMO and LUMO energies and energy gaps of D1 in neutral state

Bond/angle name	HF/3-21G*	HF/6-31G(*d*)	B3LYP/3-21G*	B3LYP/6-31G(*d*)
C_2–C_3, Å	1.328	1.330	1.361	1.363
C_1–N_1, Å	1.388	1.382	1.396	1.387
C_2–N_1, Å	1.421	1.416	1.435	1.429
C_3–N_2, Å	1.421	1.416	1.433	1.427
C_4–N_2, Å	1.388	1.381	1.393	1.385
C_5–N_2, Å	1.410	1.408	1.424	1.419
C_5–C_6, Å	1.407	1.405	1.419	1.413
C_6–N_1, Å	1.411	1.407	1.418	1.413
$N_1C_2C_3N_2$, deg	0.044	0.023	0.281	–0.017
$N_2C_5C_6N_1$, deg	0.290	0.496	1.366	1.188
$C_2C_3N_2C_5$, deg	20.555	29.268	18.723	26.715
$C_1N_1C_2$, deg	118.64	118.47	118.47	118.35
$C_3N_2C_4$, deg	118.65	118.48	118.66	118.48
$C_5N_2C_3$, deg	118.37	117.05	119.03	118.00
$C_6N_1C_2$, deg	118.41	117.14	119.21	118.24
E_{LUMO}, eV	1.5284	1.5959	–2.1197	–2.1270
E_{HOMO}, eV	–5.1543	–5.2702	–3.5050	–3.5592
ΔE, eV	6.6827	6.8661	1.3853	1.4321

Table 4. Molecular geometry, bond distances, bond angles, torsional angles, the calculated HOMO and LUMO energies and energy gaps of BCP in neutral state

Bond/angle name	HF/3-21G*	HF/6-31G(*d*)	B3LYP/3-21G*	B3LYP/6-31G(*d*)
C_2–C_3, Å	1.449	1.459	1.454	1.460
N_1–N_2, Å	2.746	2.712	2.744	2.717
C_1–N_1, Å	1.307	1.298	1.334	1.324
C_2–N_1, Å	1.345	1.343	1.360	1.353
C_3–N_2, Å	1.345	1.343	1.360	1.353
C_4–N_2, Å	1.307	1.298	1.334	1.324
$N_1C_2C_3N_2$, deg	0.000	0.000	0.000	0.000
$C_7C_1N_1C_2$, deg	0.334	0.637	0.712	0.917
$C_8C_4N_2C_3$, deg	–0.334	–0.637	–0.712	–0.917
$C_1N_1C_2$, deg	120.47	119.38	119.23	118.80
$C_3N_2C_4$, deg	120.47	119.38	119.23	118.80
$C_6C_1N_1$, deg	118.30	117.86	117.60	117.31
$C_5C_4N_2$, deg	118.30	117.86	117.60	117.31
E_{LUMO}, eV	2.4704	2.4351	–1.2947	–1.2849
E_{HOMO}, eV	–7.9804	–7.7556	–5.9385	–5.7869
ΔE, eV	10.4509	10.1907	4.6438	4.5020

Table 5. Molecular geometry, bond distances, bond angles, torsional angles, the calculated HOMO and LUMO energies and energy gaps of $IM2^+$ in neutral state

Bond/angle name	HF/3-21G*	HF/6-31G(*d*)	B3LYP/3-21G*	B3LYP/6-31G(*d*)
C_2–C_3, Å	0	1.458	1.451	1.457
N_1–N_2, Å	2.866	2.866	2.854	2.864
C_1–N_1, Å	1.305	1.297	1.333	1.324
C_2–N_1, Å	1.343	1.341	1.354	1.349
C_3–N_2, Å	1.386	1.390	1.395	1.398
C_4–N_2, Å	1.346	1.340	1.370	1.364
C_6–N_2, Å	1.474	1.464	1.481	1.469
C_7–C_1, Å	3.079	3.090	3.091	3.115
$N_1C_2C_3N_2$, deg	–1.434	–12.163	–4.700	–9.929
$C_1N_1C_2$, deg	121.41	120.10	120.22	119.69
$C_3N_2C_4$, deg	121.61	121.20	121.65	121.44
$C_6N_2C_3$, deg	123.24	122.87	123.18	123.26
$C_8C_1N_1$, deg	118.91	118.46	118.14	117.84
$C_5C_4N_2$, deg	120.42	121.06	119.85	120.51
E_{LUMO}, eV	–2.1485	–2.0527	–5.5540	–5.4715
E_{HOMO}, eV	–9.6958	–9.4498	–7.6092	–7.4615
ΔE, eV	7.5472	7.3970	2.0552	1.9899

Table 6. Molecular geometry, bond distances, bond angles, torsional angles, the calculated HOMO and LUMO energies and energy gaps of D2 in neutral state

Bond/angle name	HF/3-21G*	HF/6-31G(*d*)	B3LYP/3-21G*	B3LYP/6-31G(*d*)
C_2–C_3, Å	1.324	1.328	1.357	1.361
C_1–N_1, Å	1.402	1.401	1.416	1.407
C_2–N_1, Å	1.423	1.417	1.436	1.430
C_3–N_2, Å	1.423	1.416	1.437	1.429
C_4–N_2, Å	1.402	1.401	1.407	1.405
C_6–N_2, Å	1.417	1.416	1.433	1.427
C_6–C_7, Å	1.405	1.402	1.416	1.410
C_7–N_1, Å	1.417	1.415	1.423	1.423
$N_1C_2C_3N_2$, deg	0.028	0.036	0.054	–0.082
$N_1C_7C_6N_2$, deg	0.293	0.432	0.513	0.837
$C_5C_4N_2C_6$, deg	35.300	–50.815	–36.703	–50.714
$C_8C_1N_1C_7$, deg	–35.245	–50.993	44.726	50.476
$C_1N_1C_2$, deg	118.02	117.76	117.95	117.81
$C_3N_2C_4$, deg	118.05	117.79	118.12	117.87
$C_8C_1N_2$, deg	118.91	117.67	118.42	117.92
$C_5C_4N_2$, deg	118.93	117.69	119.25	117.95
$C_2N_1C_7$, deg	115.37	113.15	115.61	113.94
$C_3N_2C_6$, deg	115.32	113.03	115.43	113.67
E_{LUMO}, eV	–1.6062	–1.6049	–2.0138	–2.0555
E_{HOMO}, eV	–5.2773	–5.5216	–3.5885	–3.7124
ΔE, eV	3.6710	3.9167	1.5747	1.6568

a neutral state [23]. The potential energy curve of this reaction is shown in Fig. 8 [22].

The hopping rates for the self-exchange reactions are given by Eq. (1), the semi-classical Marcus theory [24–28]

$$k_{et} = \left(\frac{4\pi^2}{h}\right)\Delta H_{ab}^2(4\pi\lambda_{\pm}T)^{-\frac{1}{2}}e^{\frac{-\lambda_{\pm}}{4k_BT}}. \quad (1)$$

Here, $\lambda_{\pm}$ are reorganization energies, ΔH_{ab} is the electronic coupling matrix element between donor and acceptor k_B is the Boltzman constant, and h is the Planck constant [24–28].

The reorganization energies are purely intrinsic properties of a single molecule and these energies consists of four terms corresponding to the structural relaxation energies λ_1, λ_2, λ_3 and λ_4 [22]. The sum of the relaxation energies λ_1 and λ_2 toward optimum geometries is the reorganization energy, λ_+, for the hole transport process and the sum of the relaxation energies λ_3 and λ_4 toward optimum geometries is the reorganization energy, λ_-, for the electron transport process [22].

In the reorganization process λ_1, the geometry changes from the optimized neutral state to the optimized cationic state while the compound is in its cationic state [22]. In the λ_2 process, the geometry change is the reverse of λ_1 while the compound is in its neutral state [22]. Because these two processes involve the same geometrical change, it is reasonable to expect that λ_1 and λ_2 to be comparable. Accordingly, the reorganization energies λ_3 and λ_4 should be similar [22].

Table 7. Bond distances, bond angles and torsional angles of BPhen in cationic and anionic states, calculated by the DFT/B3LYP method with the 6-31G(*d*) basis set

Bond/angle name	Cationic	Anionic
C_2–C_3, Å	1.473	1.477
N_1–N_2, Å	2.710	2.710
C_1–N_1, Å	1.339	1.340
C_2–N_1, Å	1.330	1.340
C_3–N_2, Å	1.330	1.340
C_4–N_2, Å	1.339	1.340
$N_1C_2C_3N_2$, deg	0.000	0.000
$C_1N_1C_2$, deg	117.92	118.02
$C_3N_2C_4$, deg	117.92	118.02

Table 8. Bond distances, bond angles and torsional angles of BCP in cationic and anionic states, calculated by the DFT/B3LYP method with the 6-31G(*d*) basis set

Bond/angle name	Cationic	Anionic
C_2–C_3, Å	1.478	1.478
N_1–N_2, Å	2.710	2.710
C_1–N_1, Å	1.350	1.345
C_2–N_1, Å	1.326	1.338
C_3–N_2, Å	1.326	1.338
C_4–N_2, Å	1.350	1.345
$N_1C_2C_3N_2$, deg	0.000	0.000
$C_7C_1N_1C_2$, deg	0.458	2.089
$C_8C_4N_2C_3$, deg	–0.458	–2.089
$C_1N_1C_2$, deg	118.90	118.91
$C_3N_2C_4$, deg	118.90	118.91
$C_6C_1N_1$, deg	115.86	116.04
$C_5C_4N_2$, deg	115.86	116.04

Table 9. Bond distances, bond angles and torsional angles of D1 in cationic and anionic states, calculated by the DFT/B3LYP method with the 6-31G(*d*) basis set

Bond/angle name	Cationic	Anionic
C_2–C_3, Å	1.382	1.395
C_1–N_1, Å	1.407	1.374
C_2–N_1, Å	1.434	1.405
C_3–N_2, Å	1.427	1.405
C_4–N_2, Å	1.394	1.374
C_5–N_2, Å	1.410	1.427
C_5–C_6, Å	1.434	1.407
C_6–N_1, Å	1.382	1.424
$N_1C_2C_3N_2$, deg	–0.479	0.124
$N_2C_5C_6N_1$, deg	3.798	0.961
$C_2C_3N_2C_5$, deg	25.251	16.655
$C_1N_1C_2$, deg	117.71	119.16
$C_3N_2C_4$, deg	118.42	119.19
$C_5N_2C_3$, deg	118.87	119.21
$C_6N_1C_2$, deg	119.82	119.27

Table 11 shows reorganization energies λ_+ and λ_- of BPhen, BCP, D1 and D2 dimers plus their components λ_1, λ_2, λ_3 and λ_4.

The values of λ_1 and λ_2 are nearly equal for the monomers and the D1 dimer but are quite different for the D2 dimer. The magnitudes of λ_3 and λ_4 for the monomers and the dimers are nearly equal.

The large difference between λ_1 and λ_2 for the D2 dimer can be explained by investigating geometrical changes in its anionic and cationic states.

When the D2 dimer state changes from neutral to cationic, its torsional angles $C_5C_4N_2C_6$, $C_8C_1N_1C_7$ and $N_1C_2C_3N_2$ change from –50.714° to –29.608°, 50.476° to 29.353° and –0.082° to 0.019° respectively and the C_4–N_2 and C_1–N_1 bonds are strengthened (Table 6 and 10). This bond strengthening impedes the relaxation of the $C_5C_4N_2C_6$ and $C_8C_1N_1C_7$ torsional angles. However, the C_2–C_3 bond is weakened, aiding the relaxation of $N_1C_2C_3N_2$ torsional angle. These torsional angle changes are highly significant and are dominant factors in determining λ_1 and λ_2 energies.

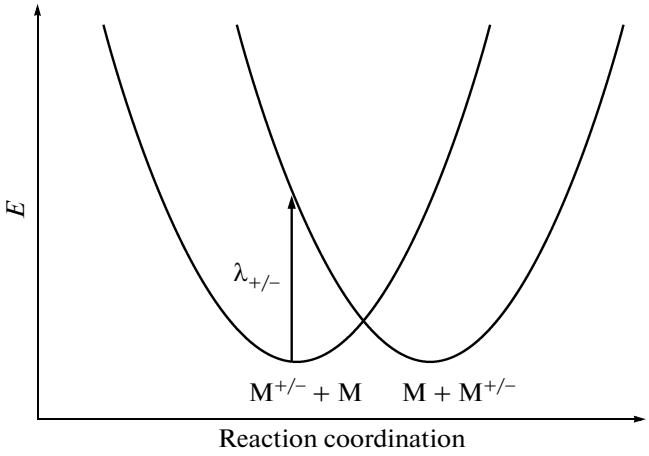

Fig. 8. Schematic diagram in the transitions for the hole and electron transports [22].

In the λ_2 process, the energy required to reorganize $C_5C_4N_2C_6$ and $C_8C_1N_1C_7$ angles is greater than the energy required in the λ_1 process.

When the D2 dimer state changes from neutral to anionic, its torsional angles $C_5C_4N_2C_6$, $C_8C_1N_1C_7$ and $N_1C_2C_3N_2$ change from –50.714° to –55.442°, 50.476° to 50.004° and –0.082° to 0.0708° respectively (Table 6 and 10). These angle changes are negligible.

There is a minor difference between λ_1 and λ_2 in the D1 dimer. For the D1 dimer in its cationic state, the C_3–N_2 bond is weakened and this bond weakening will facilitate the $C_2C_3N_2C_5$ angle to change from 26.715° to 16.655°.

There is a small difference between λ_3 and λ_4 in the BCP monomer. For the BCP monomer in its anionic state, the C_1–N_1 bond is weakened and this bond weakening will facilitate the dihedral angle $C_7C_1N_1C_2$ to change from 0.917° to 2.089°.

If one assumes T to be 298.15 K and neglects the small differences in ΔH_{ab} for electrons and holes, then a modified form of Eq. (1) will be [17]:

$$k_{et} = (\lambda_+/\lambda_-)^{1/2}\exp[(\lambda_+ - \lambda_-)/(4k_B T)]. \quad (2)$$

Table 10. Bond distances, bond angles, and torsional angles of D2 in cationic and anionic states, calculated by the DFT/B3LYP method with the 6-31G(*d*) basis set

Bond/angle name	Cationic	Anionic
C_2–C_3, Å	1.375	1.393
C_1–N_1, Å	1.421	1.388
C_2–N_1, Å	1.435	1.410
C_3–N_2, Å	1.434	1.410
C_4–N_2, Å	1.418	1.387
C_6–N_2, Å	1.413	1.430
C_6–C_7, Å	1.420	1.406
C_7–N_1, Å	1.399	1.428
$N_1C_2C_3N_2$, deg	–0.708	0.019
$N_1C_7C_6N_2$, deg	2.227	0.828
$C_5C_4N_2C_6$, deg	–55.442	–29.608
$C_8C_1N_1C_7$, deg	50.004	29.353
$C_1N_1C_2$, deg	117.65	119.34
$C_3N_2C_4$, deg	117.74	119.39
$C_8C_1N_1$, deg	117.57	120.51
$C_5C_4N_2$, deg	117.46	120.54
$C_2N_1C_7$, deg	115.52	115.78
$C_3N_2C_6$, deg	114.56	115.63

Table 11 shows the relative hopping rates, (k_{et-}/k_{et+}), of electrons over holes calculated using the Eq. (2).

The relative hopping rates data show that the dimerization reaction of the BCP monomer causes degradation of the electron transporting BCP under hole transporting conditions. The reason for this degradation is because the relative hopping rates of the D2 dimer is larger than its monomer and increases as the amount of phenyl rings in the D2 dimer increases.

The relative hopping rates of the D1 dimer is smaller than its monomer and decreases as the amount of phenyl rings in the D1 dimer increases. The calculations show that the order of k_{et-}/k_{et+} is D2 > BPhen > BCP > D1 and thus the presence of methyl groups in the D1 and D2 dimers seems to make the k_{et-}/k_{et+} value to be lowest and highest, respectively.

Table 11 shows the magnitude of λ_- is larger than λ_+ for all compounds except for the D2 dimer. The value of λ_- for the BCP monomer is larger than λ_- of the BPhen monomer and λ_- of the D1 dimer is larger than the λ_- of the BPhen monomer but the value of the D2 dimer is smaller than the λ_- of the BCP monomer. These results show that the methyl groups and the phenyl rings act as sterically hindering groups.

3.3. Ionization Potential and Electron Affinity

Ionization potentials (IP), Electron Affinities (EA), Re-organization energies λ_+ and λ_-, together with its Components, λ_1, λ_2, λ_3 and λ_4, calculated by the DFT/B3LYP method with the 6-31G(*d*) basis set are given in Table 11.

The higher IP of the BPhen monomer compared to that of the BCP monomer is due to the electron donating effect of the methyl groups in the BCP monomer.

The magnitudes of IP for the dimers are smaller than the IP values for their monomers. The values of IP (7.37 and 7.15 eV) and ΔE (4.50 and 4.50 eV) for the BPhen and the BCP monomers are large compared with values of IP (4.74 and 4.87 eV) and ΔE (1.43 and 1.65 eV) for the D1 and D2 dimers.

The slightly smaller EA of the BCP monomer than that of the BPhen monomer shows that the methyl groups are effective in lowering EA. The magnitudes of EA and HOMO energies for the dimers are larger than the corresponding magnitudes in their monomers but the magnitudes of IP and LUMO for the monomers are larger than the corresponding magnitudes in their dimers.

3.4. Thermodynamic Properties

Table 12 shows Zero-point vibrational energy, entropy, sum of electronic and thermal free energy, sum of electronic and thermal enthalpy and total energy were obtained for the monomers, positively charged intermediates and the dimers at the

Table 11. Relative hopping rates of electron over hole, Ionization potentials (IP) Electron Affinities (EA), Reorganization energies λ_+ and λ_-, together with its Components, λ_1, λ_2, λ_3, and λ_4, calculated by the DFT/B3LYP method with the 6-31G(*d*) basis set

	k_{et-}/k^{a}_{et+}	IP, eV	EA, eV	λ_1, eV	λ_2, eV	λ_+, eV	λ_3, eV	λ_4, eV	λ_-, eV
BPhen	0.5267	7.3693	0.1081	0.1615	0.1617	0.3232	0.1836	0.1970	0.3806
BCP	0.4904	7.1567	–0.0165	0.1798	0.1874	0.3672	0.1953	0.2368	0.4321
D1	0.4410	4.7452	1.0511	0.1480	0.1702	0.3182	0.2005	0.1912	0.3917
D2	6.1009	4.8778	0.9764	0.2170	0.3148	0.5318	0.1808	0.1841	0.3649

[a] Calculated for 298.15 K, neglecting differences in ΔH_{ab}.

Table 12

	HF/3-21G*	HF/6-31G(*d*)	B3LYP/3-21G*	B3LYP/6-31G(*d*)
	225.9683[a]	223.9130[a]	210.4390[a]	208.9489[a]
	139.641[b]	139.247[b]	141.657[b]	142.845[b]
Bphen	−1021.0304[c]	−1026.7817[c]	−1027.7309[c]	−1033.4338[c]
	−1020.9640[d]	−1026.7156[d]	−1027.6636[d]	−1033.3660[d]
	−1021.3421[e]	−1027.0908[e]	−1028.0182[e]	−1033.7186[e]
	446.9160[a]	442.8486[a]	416.0583[a]	413.281[a]
	234.933[b]	234.201[b]	240.202[b]	241.464[b]
$IM1^+$	−2041.2902[c]	−2052.6674[c]	−2054.5404[c]	−2065.9331[c]
	−2041.1786[d]	−2052.7787[d]	−2054.6545[d]	−2066.04792[d]
	−2041.9267[e]	−2053.4098[e]	−2055.2420[e]	−2066.6310[e]
	438.8049[a]	434.8987[a]	407.8433[a]	405.096[a]
	226.031[b]	226.822[b]	234.050[b]	234.283[b]
D1	−2054.2251[c]	−2052.2115[c]	−2054.2251[c]	−2065.4985[c]
	−2040.8409[d]	−2052.3192[d]	−2054.1139[d]	−2065.6098[d]
	−2041.4680[e]	−2052.9406[e]	−2054.8018[e]	−2066.1827[e]
	262.4633[a]	260.3569[a]	244.9912[a]	243.2672[a]
	156.704[b]	157.184[b]	159.531[b]	161.633[b]
BCP	1098.6277[c]	−1104.8106[c]	−1105.8971[c]	−1111.9498[c]
	−1098.5532[d]	−1104.7360[d]	−1105.8213[d]	−1112.0266[d]
	−1098.9931[e]	−1105.1729[e]	−1106.2347[e]	−1112.3610[e]
	520.3266[a]	516.089[a]	485.4428[a]	482.1507[a]
	266.428[b]	266.833[b]	273.414[b]	277.313[b]
$IM2^+$	−2196.4857[c]	−2208.7067[c]	−2210.9895[c]	−2223.2332[c]
	−2196.3591[d]	−2208.8335[d]	−2210.8596[d]	−2223.1014[d]
	−2197.2312[e]	−2209.5728[e]	−2211.6791[e]	−2223.9164[e]
	512.0578[a]	508.5772[a]	477.0269[a]	474.3969[a]
	258.224[b]	258.916[b]	269.924[b]	267.711[b]
D2	−2195.8941[c]	−2208.3593[c]	−2210.5408[c]	−2222.7780[c]
	−2196.0168[d]	−2208.2363[d]	−2210.4126[d]	−2222.6508[d]
	−2196.7524[e]	−2209.0897[e]	−2211.2181[e]	−2223.4525[e]

[a] Zero-point vibrational energy (Kcal mol^{-1}), [b] entropy (cal mol^{-1} K^{-1}), [c] sum of electronic and thermal free energy (hartree), [d] sum of electronic and thermal enthalpy (hartree) and [e] total energy (hartree).

HF/3-21G*, HF/6-31G(*d*), B3LYP/3-21G* and B3LYP/6-31G(*d*) levels of ab initio method. The thermodynamic properties, calculated at the same level of ab initio method with different basis sets, are only slightly different. Total energies and triplet energies of excited positively charged monomers are given in Table 13. Table 14 exhibits relative total energies (relative to the reactants) for reactions (1) and (2) at the levels of HF/3-21G*, HF/6-31G(*d*), B3LYP/3-21G* and B3LYP/6-31G(*d*). The energy variation in the reactions (1) and (2), calculated by the B3LYP/6-31G(*d*) method, is depicted in Fig. 9. This figure shows that total energies of IM1, IM2, P1 and P2 are 22.20, 26.66, 303.50 and 313.77 kcal mol^{-1} and they are higher than the total energies of their reactants R1 and R2. It is clear that the different methods predict different values and since there are no experimental data are available for all compounds to be compared with our theoretical results (Tables 12–14), hence, we consider the present results with B3LYP/6-31G(*d*) are more accurate, DFT methods such as B3LYP/6-31G(*d*) are often times considered to be standard model chemistry for many applications. We hope that our present work will stimulate some more works on these materials. Future experimental works will testify our calculated results.

Table 13. Total energies and excitation energies for excited positively charged monomers (BPhen*+ and BCP*+) at td-triplets

	HF/3-21G*	HF/6-31G(*d*)	B3LYP/3-21G*	B3LYP/6-31G(*d*)
BPhen*+	−1021.0704[a]	−1026.8446[a]	1027.7371[a]	−1033.4477[a]
	−2.2282[b]	−2.2783[b]	0.0999[b]	0.3903[b]
BCP*+	−1098.7269[a]	−1104.9332[a]	−1105.9612[a]	−1112.0979[a]
	−2.3957[b]	−2.3076[b]	0.0916[b]	0.4114[b]

[a] Total energies (Hartree) and [b] bexcitation energies (eV).

Table 14. Relative total energies (relative to the reactants) for reactions (1) and (2), at the levels of HF/3-21G*, HF/6-31G(*d*), B3LYP/3-21G* and B3LYP/6-31G(*d*), in eV

	HF/3-21G*	HF/6-31G(*d*)	B3LYP/3-21G*	B3LYP/6-31G(*d*)
R1	0.00	0.00	0.00	0.00
IM1	−0.2827	0.7452	0.4356	0.9627
P1	12.1989	13.5126	12.4139	13.1609
R2	0.00	0.00	0.00	0.00
IM2	−0.2010	0.9542	0.5303	1.1564
P2	12.8384	14.0998	13.0745	13.7796

3.5. Conclusion

This theoretical work has helped us to gain further insight into the dimerization reactions of the BPhen and the BCP. The optimization of geometry calculations depend on the initial geometry around nitrogen atoms in the BPhen and the BCP reactants and their products. The variations in the geometries can be seen from HOMO and LUMO energies. The BPhen and the BCP dimers have the lowest LUMO energy levels in comparison with the LUMO energy levels for the BPhen and the BCP monomers and this is due to the dimers expanded *p*-electron system.

The reorganization energy λ_- of BPhen, BCP, BPhen intermediate, BCP intermediate and BPhen dimer is larger than λ_+, except for the BCP dimer. The magnitudes of HOMO and EA for the dimers are larger than the corresponding values in their monomers. The magnitudes of LUMO, IP and energy gap for the monomers are larger than the corresponding values in their dimers. The magnitudes of λ_- for the BPhen monomer is smaller than its λ_- for the BPhen dimer and λ_- of the BCP monomer is larger than λ_- of the BCP dimer. In contrast, the magnitude of λ_+ of the BPhen monomer is larger than its λ_+ value of the BPhen dimer and λ_+ value of the BCP monomer is smaller than its value in the BCP dimer. The relative hopping rates of electrons over holes for the BCP dimer is larger than its rate for its monomer, but for the BPhen dimer is smaller than its monomer.

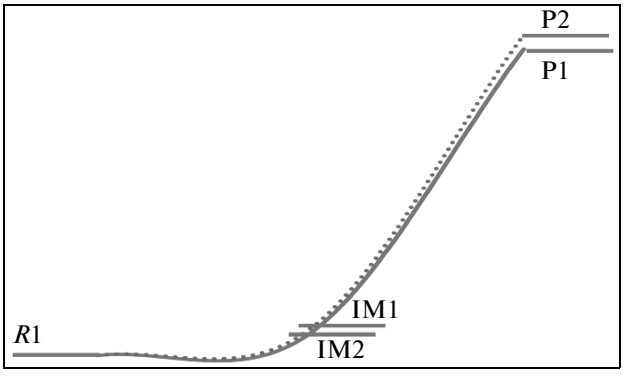

Fig. 9. Schematic energy profile of the reactions (P1) and (P2) calculated by B3LYP/6-31G method.

Our results show that not only the methyl group, but also the phenyl rings act as sterically hindering groups and the generation of the BCP dimer is less pronounced than the BPhen dimer. The electron transport rate of the BPhen monomer is slightly higher than that of the BCP monomer. The electron transport rate of the BPhen dimer is much higher than that of the BCP monomer and the electron transport rate of the BCP dimer is lower than that of the BPhen monomer.

ACKNOWLEDGMENTS

This work was supported by Graduate University of Advanced Technology and Research Center for Science, High Technology & Environmental Science. This article was peer reviewed by Nasser Mirzai-Baghini, Imperial College Reactor Centre, Silwood Park, Ascot, Berkshire, United Kingdom.

REFERENCES

1. A. R. Duggal, J. J. Shiang, C. M. Heller, and D. F. Foust, Appl. Phys. Lett. **80**, 3470 (2002).
2. S. R. Forrest, Nature (London) **428**, 911 (2004).
3. Y. Shirota, K. Okumoto, and H. Inada, Synth. Met. **387**, 111 (2000).
4. B. C. Maiti, S. Z. Wang, C. P. Cheng, D. J. Huang, and C.-I. Chao, Chin. Chem. Soc. **48**, 1059 (2001).
5. S. Sebastian S. C. Cathrin, W. Karsten, K. Dirk, and L. Karl, Org. Electron. **8**, 709 (2007).
6. H. Aziz and Z. D. Popovic, Chem. Mater. **16**, 4522 (2004).
7. H. Aziz, Z. D. Popovic, N. Hu, A. Hor, and G. Xu, Science **283**, 1900 (1999).
8. Z. D. Popovic, H. Aziz, N.-X. Hu, A. Ioannidis, and P. N. M. dos Anjos, J. Appl. Phys. **89**, 4673 (2001).
9. F. Steuber, J. Staudigel, M. Stössel, J. Simmerer, A. Winnacker, H. Spreitzer, F. Weissörtel, and J. Salbeck, Adv. Mater. **12**, 130 (2000).
10. M. Müller-Wiegand, G. Georgiev, E. Oesterschulze, T. Fuhrmann, and J. Salbeck, Appl. Phys. Lett. **81**, 4940 (2002).
11. S. T. Lee, Z. Q. Gao, and L. S. Hung, Appl. Phys. Lett. **75**, 1404 (1999).
12. M. Scharnberg, J. Hu, J. Kanzow, K. Ratzke, R. Adelung, F. Faupel, C. Pannemann, U. Hilleringmann, S. Meyer, and J. Pflaum, Appl. Phys. Lett. **86**, 024104 (2005).
13. W. Song, Z. Li, S. K. So, Y. Qiu, Y. Zhu, and L. Cao, Surf. Interface Anal. **32**, 102 (2001).
14. M. J. Frisch, G. W. Trucks, H. B. Schlegel, et al., *Gaussian 03* (Gaussian Inc., Pittsburgh PA, 2003).
15. R. E. Stratmann, G. E. Scuseria, and M. J. Frisch, J. Chem. Phys. **109**, 8218 (1998).
16. S. Gao, Comput. Phys. Commun. **153**, 190 (2003).
17. K. Schwarz, J. Solid State Chem. **176**, 319 (2003).
18. B. B. Karki, L. Stixrude, S. J. Clark, M. C. Warren, G. J. Ackland, and J. Crain, Am. Mineralog. **82**, 635 (1997).
19. Li Zong-You, T. Shin-Rong, Ch. Yu-Chiang, et al., Synth. Met. **161**, 426 (2011).
20. A. Kahn, N. Koch, and W. Gao, J. Polym. Sci. B: Polym. Phys. **41**, 2529 (2003).
21. H. Bassler, Phys. Status Solidi B **175**, 15 (1993).
22. B. C. Lin, C. P. Cheng, and Z. P. M. Lao, J. Phys. Chem. A **107**, 5241 (2003).
23. H. P. Young, Y.-H. Kim, S. K. Kwon, I. S. Koo, and K. Yang, Bull. Korean Chem. Soc. **31**, 1649 (2010).
24. R. A. Marcus, J. Chem. Phys. **24**, 966 (1956).
25. R. A. Marcus, J. Chem. Phys. **43**, 679 (1965).
26. M. D. Newton and N. Sutin, Ann. Rev. Phys. Chem. **35**, 437 (1984).
27. R. A. Marcus and N. Sutin, Biochim. Biophys. Acta **811**, 265 (1985).
28. P. F. Barbara, T. J. Meyer, and M. A. Ratner, J. Phys. Chem. **100**, 13148 (1996).

SPELL: OK